


Article

An Experimental Study on the Physical and Mechanical Properties of Granite after High-Temperature Treatment Considering Anisotropy

Yan Qin ^{1,2,*} , Linqing Wu ¹, Qiong Wu ³, Nengxiong Xu ^{1,2,*}, Guanjun Cai ³, Yuxi Guo ¹ and Wenjing Zhou ¹

¹ School of Engineering and Technology, China University of Geosciences (Beijing), Xueyuan Road 29, Beijing 100083, China; 2102200102@email.cugb.edu.cn (L.W.); 3002230011@email.cugb.edu.cn (Y.G.); 3002220002@email.cugb.edu.cn (W.Z.)

² Engineering and Technology Innovation Center for Risk Prevention and Control of Major Project Geosafety, MNR, Xueyuan Road 29, Beijing 100083, China

³ Beijing Jingneng Geological Engineering Co., Ltd., 36 Mentougou Road, Mentougou District, Beijing 102300, China; wuqiongming@sina.com (Q.W.); caifeisoft@sina.com (G.C.)

* Correspondence: yanqin@cugb.edu.cn (Y.Q.); xunengxiong@cugb.edu.cn (N.X.); Tel.: +86-010-8232-3010(Y.Q.)

Abstract: The deep burial disposal of nuclear waste and dry hot rock mining relates to the effects of high temperatures on the physical and mechanical properties of granite. Previous studies have shown that due to the anisotropy of mineral arrangements during granite formation, the physical and mechanical properties of granite vary greatly with different temperatures. We conducted wave velocity tests, optical mirror tests, and uniaxial and conventional triaxial compression tests on granite in three orthogonal directions before and after high-temperature treatment. The main innovative conclusions are as follows: (1) High temperatures can cause the density of thermal cracks in the cross-section of granite, which varies with different sampling directions. Temperatures below 400 °C increase the anisotropy of granite, and there are obvious advantages in the development direction. (2) Under the same temperature conditions, granite samples taken parallel to the dominant direction of cracks exhibit the best mechanical properties. (3) In uniaxial compression tests, granite samples after high-temperature treatment are mostly subjected to tensile splitting failure. When the heating temperature is higher than 400 °C, a large number of transgranular cracks are generated during the thermal damage of granite at this temperature stage. Rock samples taken perpendicular to the dominant direction of the crack can generate radial cracks near the main failure surface, while rock samples taken parallel to the dominant direction of the crack can generate more axial cracks.

Keywords: granite; physical and mechanical properties; heat damage; anisotropy; microstructure



Citation: Qin, Y.; Wu, L.; Wu, Q.; Xu, N.; Cai, G.; Guo, Y.; Zhou, W. An Experimental Study on the Physical and Mechanical Properties of Granite after High-Temperature Treatment Considering Anisotropy. *Appl. Sci.* **2024**, *14*, 5585. <https://doi.org/10.3390/app14135585>

Academic Editor: Syed Minhaj Saleem Kazmi

Received: 5 June 2024

Revised: 24 June 2024

Accepted: 24 June 2024

Published: 27 June 2024



Copyright: © 2024 by the authors. Licensee MDPI, Basel, Switzerland. This article is an open access article distributed under the terms and conditions of the Creative Commons Attribution (CC BY) license (<https://creativecommons.org/licenses/by/4.0/>).

1. Introduction

In deep rock engineering, rocks often encounter high-temperature environments. For example, during the development of geothermal energy, the ambient temperature of dry hot rocks is above 200 °C [1,2]. In a deep burial disposal project involving high-level radioactive nuclear waste, the decay of radioactive elements in nuclear waste releases a large amount of heat, resulting in the surrounding rock being in a high-temperature environment for a long time [3,4]. In the process of engineering construction and operation, reconstruction after a building fire must also consider the impact of high temperatures on rocks [5–7]. A high temperature will significantly reduce the physical and mechanical properties of rocks, thus affecting engineering safety. Granite, a common magmatic rock, has the characteristics of low permeability, low density, and high strength and is widely used in buildings around the world. It is also the main reservoir rock for geothermal energy and the surrounding rock of deep burial disposal sites for high-level radioactive waste. Therefore, it is of great significance for engineering rock mechanics to study the physical

and mechanical properties of granite after high-temperature treatment, such as in the deep burial disposal of nuclear waste and dry hot rock mining.

A high temperature causes the thermal expansion of mineral particles inside rocks and the extensive development of microcracks, leading to the loosening of the rock structure. On a macroscopic level, it is manifested that the physical and mechanical properties of rocks will deteriorate to varying degrees after different high-temperature treatment. In recent years, scholars have conducted both domestic and international research on the physical and mechanical properties of granite after high temperature treatment and have achieved significant results. Morrow et al. [8] and Chaki et al. [9] measured the porosity and permeability of granite after different temperature treatments, and the experimental results show that the porosity and permeability of granite increase with an increasing temperature. Additionally, the physical and mechanical properties of granite deteriorate. Sun et al. [10] measured the quality of granite treated at different temperatures ranging from room temperature to 800 °C and found that the quality of the rock sample decreased with an increasing heating temperature, which was related to the loss of free and bound water in the rock minerals. Yang et al. [11] reported that the density of granite decreases with an increasing temperature, and the magnitude of the decrease increases with an increasing heating temperature. Zhu et al. [12] found, through experiments, that the longitudinal wave velocity of granite decreases with an increasing temperature, and the higher the temperature is, the faster the decrease in the longitudinal wave velocity. Zhang et al. [13] conducted a comprehensive review of previous research on the variation in granite wave velocity after high-temperature treatment and divided the trend of the granite longitudinal wave velocity with temperature into three stages: at room temperature (~150 °C), there was no significant change in the longitudinal wave velocity; at 200–600 °C, the longitudinal wave velocity rapidly decreased with an increasing temperature; and at a heat-treatment temperature above 600 °C, the rate of decrease in the longitudinal wave velocity decreased. F. E. HEUZE [14] systematically summarized the main research results on high-temperature granite before 1983, compared the research results of different scholars through normalization, obtained the variation law of the main mechanical indicators of granite with temperature, and discussed future research directions. Liu et al. [15] studied the physical and mechanical properties of granite after high-temperature treatment and found that the compressive strength and elastic modulus of granite decreased with an increase in the temperature. Compared with the static elastic modulus, the dynamic elastic modulus of granite decreased faster. These authors believe that a high temperature has a greater impact on the physical properties of granite than on its mechanical properties. Zhao et al. [16] conducted Brazilian splitting tests on granite specimens with three different particle size distributions after different temperature treatments and reported that as the particle size and heterogeneity increased, the Brazilian tensile strength of untreated granite decreased. Moreover, when the heating temperature was less than 300 °C, the tensile strength of granite specimens with different particle sizes increased, remained unchanged, and decreased. When the temperature reached 400 °C, the temperature significantly decreased.

Through extensive literature research, numerous scholars have collected their research results in the field of high-temperature granite, and data on thermal loss related to the physical and mechanical properties of granite have been extracted and organized. By extracting and organizing these data, a series of physical and mechanical indicators, such as the wave velocity, peak strength, and elastic modulus, of granite are summarized as functions of temperature. To more intuitively demonstrate the impact of high temperatures on granite, the data were normalized, as shown in Figures 1 and 2. According to previous reports, the overall trends of the variations in the longitudinal wave velocity, uniaxial compressive strength, and elastic modulus of granite with respect to temperature after exposure to high temperatures are relatively similar, but the variation trends are slightly different. According to previous reports, the overall trends of the variations in the longitudinal wave velocity, uniaxial compressive strength, and elastic modulus of granite with respect to temperature after exposure to high temperatures are relatively similar, but the variation trends are

slightly different. According to Chen et al. [17], the longitudinal wave velocity of granite does not change significantly when heated below 300 °C, while Ma et al.'s [18] experimental results suggest that the longitudinal wave velocity of granite significantly decreases when heated below 300 °C. In terms of the variation law of the uniaxial compressive strength, there are more significant differences among the achievements of different scholars. At heating temperatures below 200 °C, the uniaxial compressive strength shows three trends: an increase with the temperature [19], almost no change [20,21], and a decrease [15,22,23]. When the heating temperature exceeds 400 °C, there is also a significant difference in the rate of decrease in the uniaxial compressive strength with temperature. Alneasan [24] studied the effects of temperature on the fracture characteristics of granite under three loading modes and found that the fracture behavior is temperature-dependent and can transition from brittle to ductile. Wang [25,26] conducted cyclic loading tests on granite and used a specially designed acoustic emission testing system to monitor the thermal damage evolution of rocks in real time during heating and cooling processes. He established a thermal-damage-evolution model considering both heating and cooling processes. The numerical calculation results are in good agreement with the experimental results.

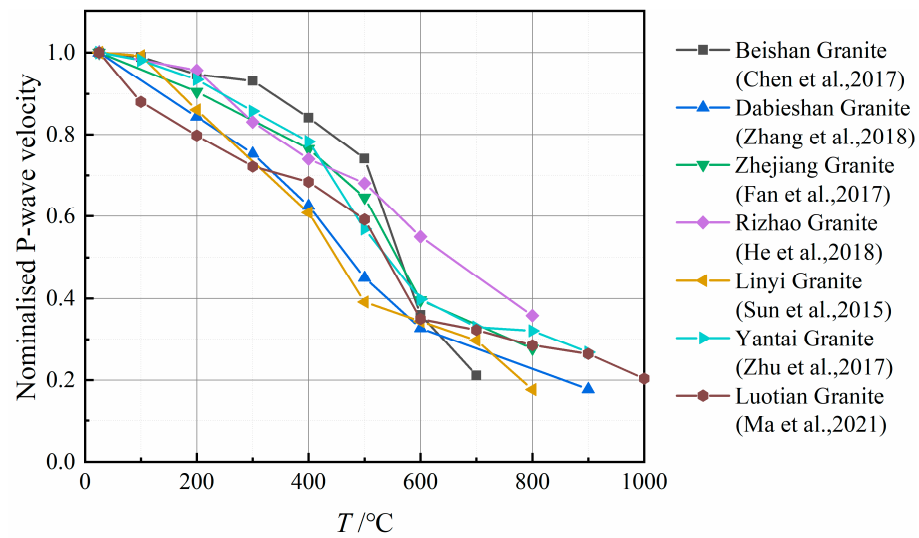


Figure 1. Normalized longitudinal wave velocity variation with different temperatures in previous studies [2,10,12,17,18,27,28].

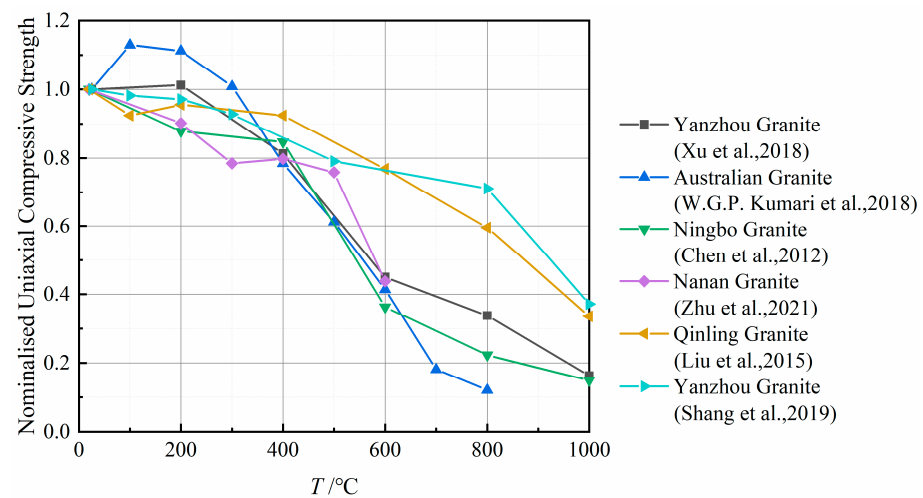


Figure 2. The variation law of the normalized uniaxial compressive strength with different temperatures in previous studies [15,19–23].

According to previous reviews, it is generally believed that the differences in the physical and mechanical properties of granite after exposure to high temperatures are due to the geological characteristics of the granite, that is, the different mineral compositions. However, this phenomenon also occurs when the mineral composition and content of the granite samples selected in the experiment are similar. Therefore, we speculate that anisotropy caused by different sampling directions is also an important influencing factor. Moreover, most scholars have conducted research on the anisotropy of granite under room-temperature conditions, with little consideration given to the effects of temperature on granite anisotropy, and there is a lack of comprehensive research on granite anisotropy.

2. Sample Preparation and Testing Steps

The granite used in the experiment was taken from Jining, Shandong Province, and had a gray-white color, was relatively fresh, and had a low degree of weathering. First, the mineral composition and microstructure of the samples were analyzed under normal temperature conditions to gain a preliminary understanding of the basic physical properties of the granite. An X-ray diffraction (XRD) analysis revealed that the main mineral components of the granite were quartz (24.4%), plagioclase (39.8%), potassium feldspar (30.6%), and biotite (5.2%).

To reduce errors and external influencing factors in the experiment, all the rock samples used in this experiment were taken from the same granite block. According to the International Society for Rock Mechanics Test Specification (ISRM 2007), all the samples were \varnothing A 50 × 100 mm cylinders. To study the anisotropy of the physical and mechanical properties of granite, samples were taken along the three orthogonal directions of granite, according to the sampling scheme in Figure 3. Seventy-two samples were processed in each direction, totaling 216 granite samples. According to the wave speed test results, the three directions are named in a descending order of the wave speed: the Z direction, X direction, and Y direction.

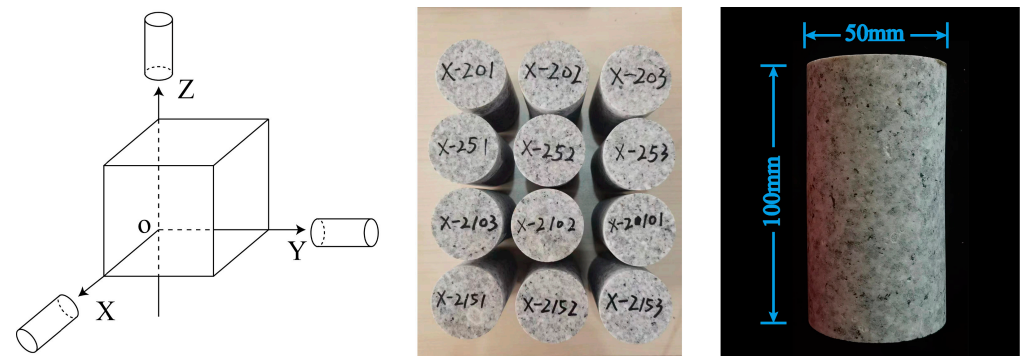


Figure 3. Sampling method and granite samples.

The heating temperature (T) was set at a temperature gradient of 200 °C and was set at 25 °C (room temperature), 200 °C, 400 °C, 600 °C, 800 °C, and 1000 °C. Uniaxial and triaxial compression tests with confining pressures of 5 MPa, 10 MPa, and 15 MPa were carried out on rock samples heated at different temperatures.

The instruments and equipment used in this experiment included electronic balances (with an accuracy of 0.001 g), vernier calipers (with an accuracy of 0.02 mm), a polarizing microscope (OLYMPUS BX53 comes from Beijing, China), an ultrasonic detector (Pundit-PL200 PE, 250 kHz comes from Beijing, China), a high-temperature furnace (SG-XL1200 comes from Beijing, China, with maximum temperature of 1200 °C and an accuracy of ± 3 °C), and a mechanical testing machine (HSW-1000B comes from Beijing, China).

The experimental procedure was as follows: The rock samples were placed in a well-ventilated place at room temperature for 2 weeks to eliminate the influence of natural moisture content. As shown in Figure 4, the rock samples were placed into a high-temperature furnace according to temperature groups for heat treatment at a heating rate of 3 °C/min.

After heating to the target temperature, the mixture was maintained at a constant temperature for 2 h. After the power was turned off, the samples were cooled naturally in the furnace to room temperature. Microscopic observation, wave velocity testing, and uniaxial and triaxial compression tests were carried out on the rock samples after high-temperature treatment, and the morphology of damaged samples was photographed.

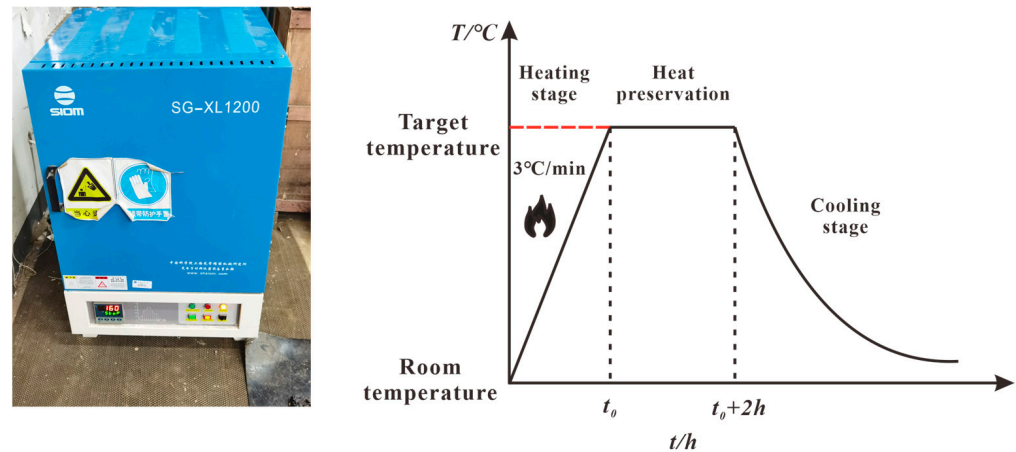


Figure 4. High-temperature furnace and rock sample heating process.

3. Test Results

The test results include the following: (1) changes in the appearance of the rock sample; (2) changes in microscopic properties; (3) changes in transverse and longitudinal wave velocities; (4) changes in the compressive strength and elastic modulus; (5) changes in cohesion and the internal friction angle; (6) anisotropic changes; and (7) destruction.

3.1. Changes in the Appearances of the Rock Samples

The surface color, tapping sound, and roughness of the granite rock samples after high-temperature treatment significantly changed compared to those of the untreated samples. Figure 5 shows the apparent color changes in some of the granite samples after being subjected to temperatures ranging from 20 °C to 1000 °C. The apparent color of the granite changed significantly with an increasing temperature. At room temperature, the granite grains appeared grayish white with a smooth surface. After heating at 200 °C, the color slightly shifted to white, and the knocking sound was crisp, indicating a smooth surface. After heating at 400 °C, the color changed to light flesh red with yellow spots, the knocking sound became turbid compared to before, and the surface was smoother. After heating at 600 °C, the overall color changed from gray to white, and the knocking sound became obviously cloudy, resulting in a rough surface. After heating at 800 °C, the white was lighter than that at 600 °C, and black substances appeared locally (which may appear on the surface where dark minerals melt and precipitate). The knocking sound was cloudy, the surface was rough, and the particles were difficult to erase. After heating at 1000 °C, the color of the granite became red compared with 800 °C, and the black material disappeared. The knock was very cloudy, and the surface was very rough and could be rubbed into particles.

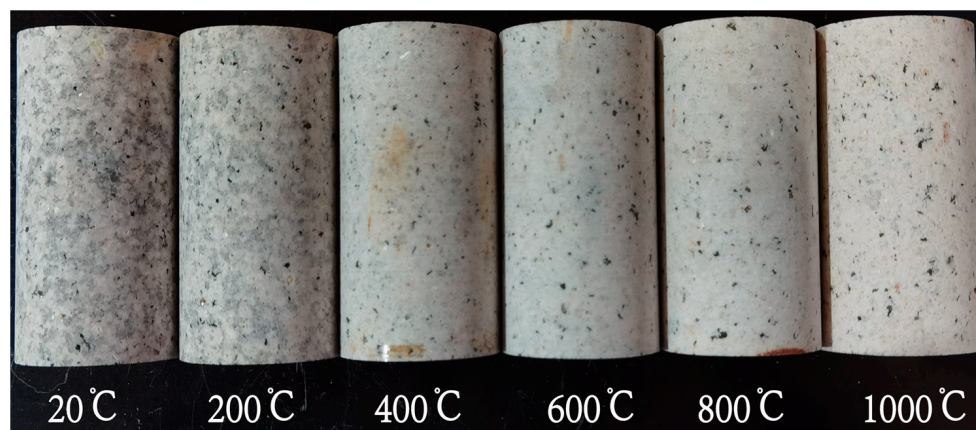


Figure 5. Comparison of granite appearance after different temperature treatments.

3.2. Changes in Microscopic Properties

As shown in Figure 6, the morphological changes in the mineral composition and microcrack-development characteristics of the granite samples after high-temperature treatment were observed using an optical microscope, and optical microscopic images of the samples treated at different temperatures were obtained. For the convenience of statistics and resolution, intergranular cracks are marked in red, intragranular cracks in the quartz are marked in yellow, intragranular cracks in the feldspar are marked in green, and intragranular cracks in the biotite are marked in orange. The rock was mainly composed of plagioclase, potassium feldspar, quartz, biotite, and a small amount of opaque minerals. In the original state, the contact edges between minerals in the rock were straight or smooth, a small number of primary cracks were observed in the quartz and feldspar crystals, and intergranular cracks were also rare. After heating at 200 °C, a small number of cracks could be observed inside the plagioclase and quartz particles, and intergranular cracks were distributed at the boundaries of the plagioclase and quartz. Compared with those in the initial state, the morphology of each mineral did not change much, but some plagioclase particles were slightly fragmented. At 400 °C, fragmentation occurred at the contact points between various minerals in the rock, with a small number of cracks appearing inside the potassium feldspar and many light brown microcracks appearing inside the quartz particles. Compared with those of the samples at room temperature, the morphology of each mineral did not change much, with biotite showing a slight reddish-brown color, indicating oxidation and obvious fragmentation within each mineral. As the heating temperature increased to 600 °C, the fragmentation phenomenon at the contact points between minerals in the rock became more pronounced than that in the sample at 400 °C, and the number of microcracks in the feldspar minerals significantly increased. Black mica exhibits a more reddish-brown color and extensive oxidation. Due to the occurrence of quartz at the 573 °C α - β phase transition, at high temperatures, (β) the volume of the phase quartz particles increased and recovered after cooling to room temperature. (α) The process of the expansion and contraction of quartz led to an increase in the number of broken minerals at the boundaries of the quartz minerals, an increase in the crack width, and an increase in the number of intergranular and intragranular cracks. After heating at 800 °C, the morphology of the various minerals changed significantly, with a large number of intergranular and intragranular cracks appearing. The fragmentation phenomenon of the internal and contact parts between minerals was more obvious. After high-temperature treatment at 1000 °C, the surfaces of the potassium feldspar, plagioclase feldspar, and quartz all became blurred, indicating strong weathering. Black mica became redder and had a greater degree of oxidation than 800 °C, while the degree of fracture of black mica was also greater. The various mineral components in the rock exhibited a large number of intragranular cracks, which were interconnected. The width of the intergranular cracks reached the maximum among all temperature levels.

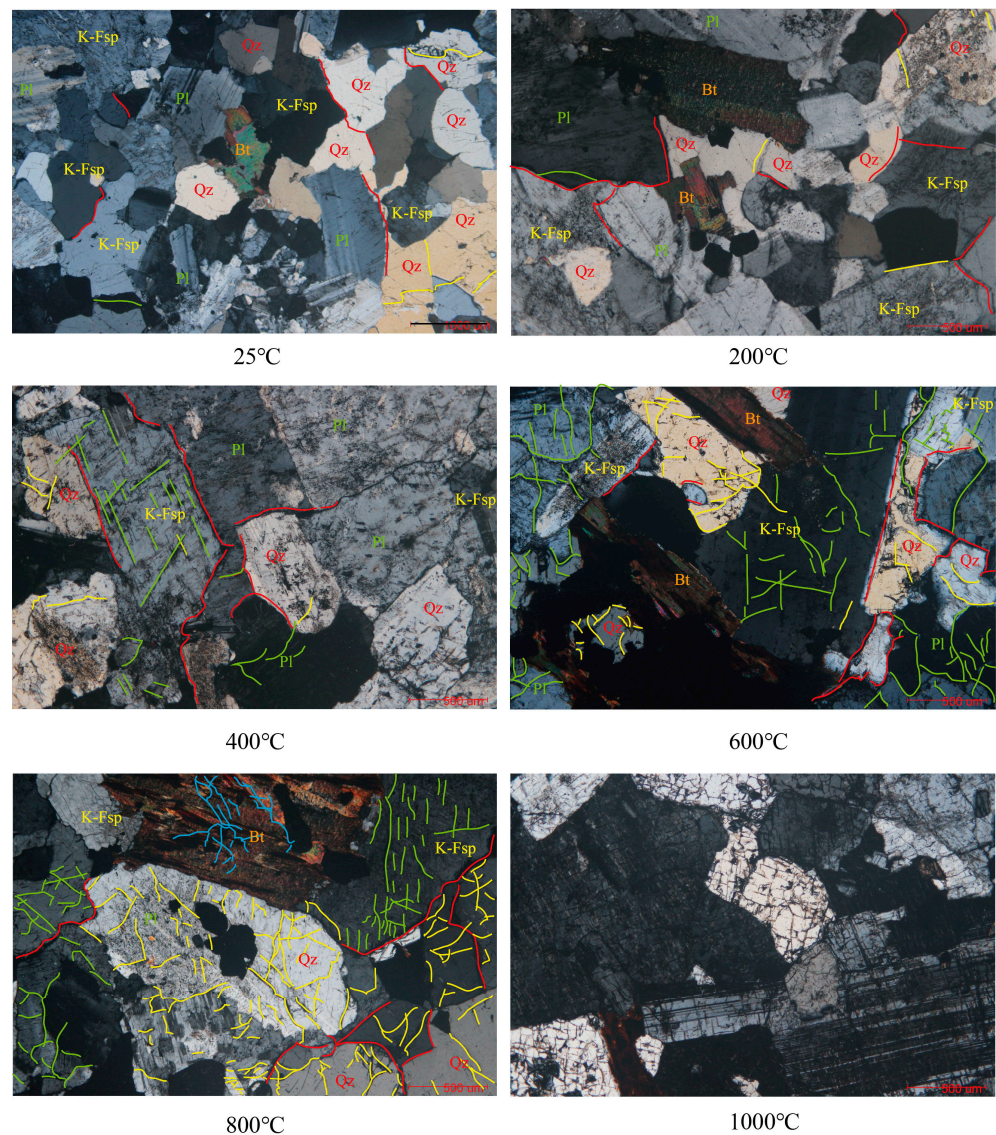


Figure 6. Microscopic images of the microstructure of granite after different temperature treatments under a polarizing microscope.

Figure 7 shows the optical microscopic images of granite samples treated at different temperatures at the same ratio, which clearly reveal the development of cracks within the rock. In the initial state, the granite had fewer primary cracks, and the surface of the mineral particles was relatively smooth. When the temperature rose to 200 °C, the granite underwent thermal damage, leading to an increase in internal cracks. However, due to an increase in the mineral volume, the primary microcracks were close to a certain extent, and their width significantly decreased. At 400 °C, the width of the intergranular cracks significantly increased, and as the temperature increased, the cracks developed and extended. Compared to those at lower temperatures, the lengths of large cracks also increased, and the number of small cracks within the crystal increased. After heating at a high temperature of 600 °C, there was a significant difference in the microstructure of the granite under the light microscope compared to the morphology at temperatures below 400 °C, with a large increase in microcracks. Wide intergranular cracks developed and connected with each other, and broken particles appeared between the minerals. A large number of microcracks within each mineral particle were derived and developed, and transgranular cracks appeared for the first time. At 800 °C, the number of cracks significantly increased, the width widened, and the length increased. The internal cracks

in the rock sample were interconnected and formed a crack network. Moreover, the small particles produced by the squeezing and crushing of minerals increased relative to those produced by lower temperature treatments. As the processing temperature increased to 1000 °C, the internal cracks in the rock sample became very dense, and the cracks became interconnected, forming a dense network of cracks. Mineral crystals were cut into small particles by these cracks. The phenomenon of particle fragmentation between minerals and within minerals was widely distributed, which can explain the significant decrease in the macroscopic mechanical properties of granite at 1000 °C.

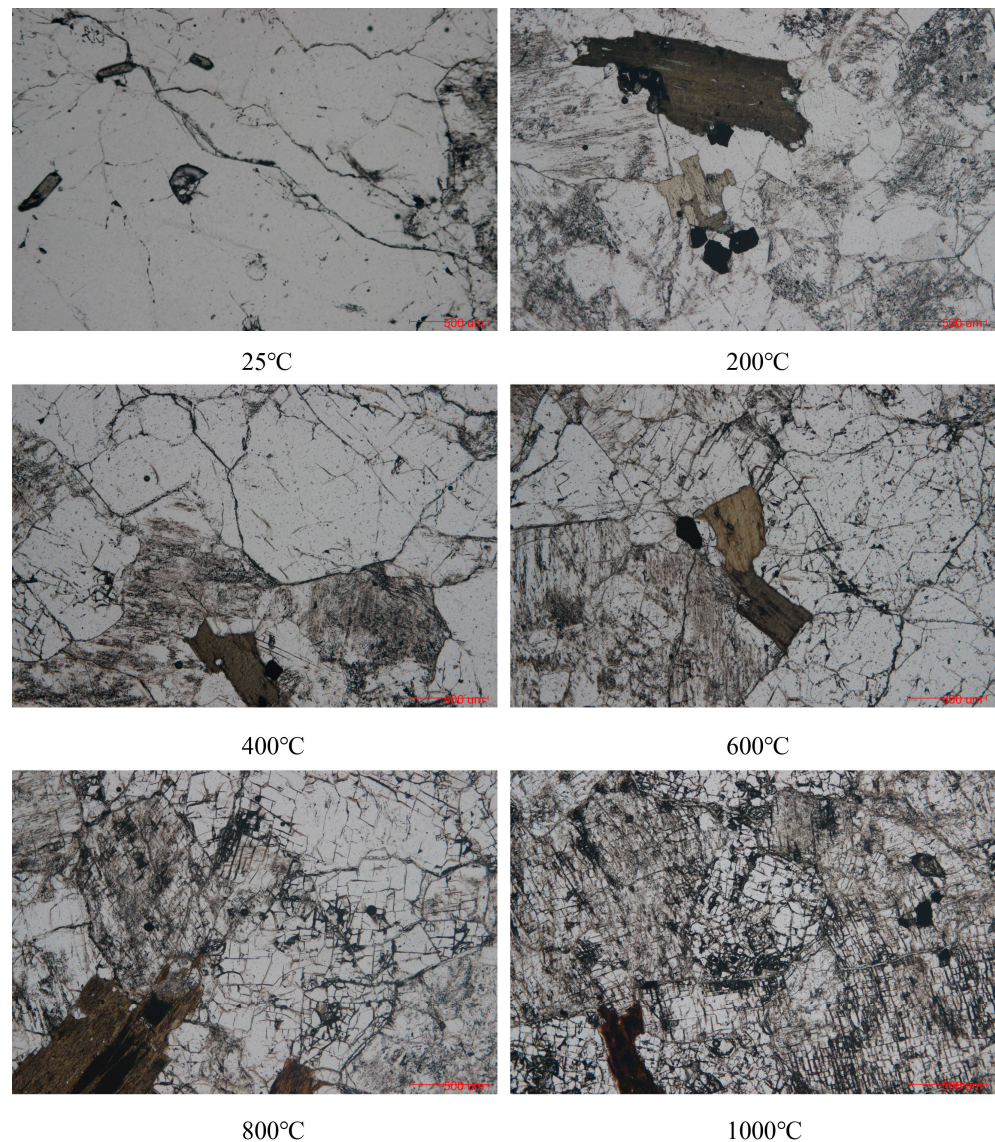


Figure 7. Crack photographs of granite sample slices after different temperature treatments.

3.3. Changes in Longitudinal and Transverse Wave Velocities

The effects of temperature on the longitudinal and transverse wave velocities of granite are shown in Figures 8 and 9, respectively. At temperatures ranging from 200 to 400 °C, the longitudinal wave velocity approximately linearly decreased, and the rate of decrease in the longitudinal wave velocity was significantly greater than that in the transverse wave velocity. At 400 °C, the longitudinal wave velocity of granite decreased to 2738 m/s, which was only 61% of that at room temperature. Although the transverse wave velocity decreased with an increasing temperature, it could still reach 76% of that at 400 °C. At 600 °C, the longitudinal wave velocity continued to decrease rapidly, with the average

longitudinal wave velocity dropping to 1312 m/s, which was only 29% of that at room temperature. The transverse wave velocity decreased significantly faster than that at 400 °C, dropping to 42% at room temperature. As the temperature continued to increase, the rate of decrease in the wave velocity slowed. At 800 °C, the longitudinal wave velocity decreased to 1009 m/s, and the transverse wave velocity decreased to 846 m/s. When the heating temperature reached 1000 °C, the ultrasonic signal became extremely chaotic and unstable, and the wave velocity could not be read anymore. There was a significant change in the wave velocity of the granite before and after 400 °C, and 400 °C can be regarded as the threshold temperature for thermal damage to the granite wave velocity.

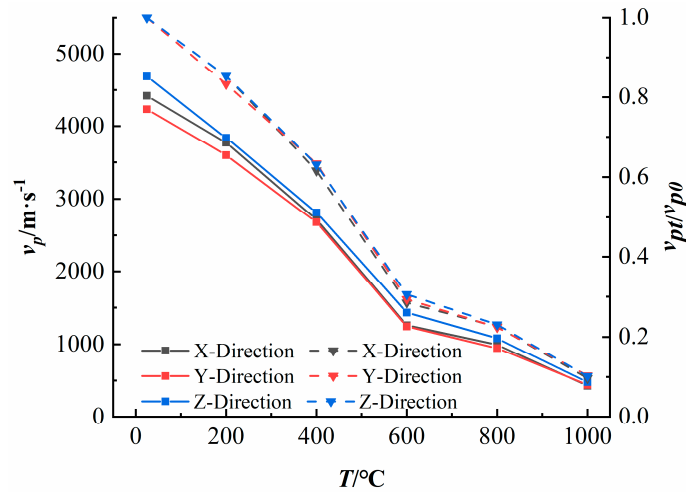


Figure 8. Temperature-dependent variation in the longitudinal wave velocity of granite in different sampling directions.

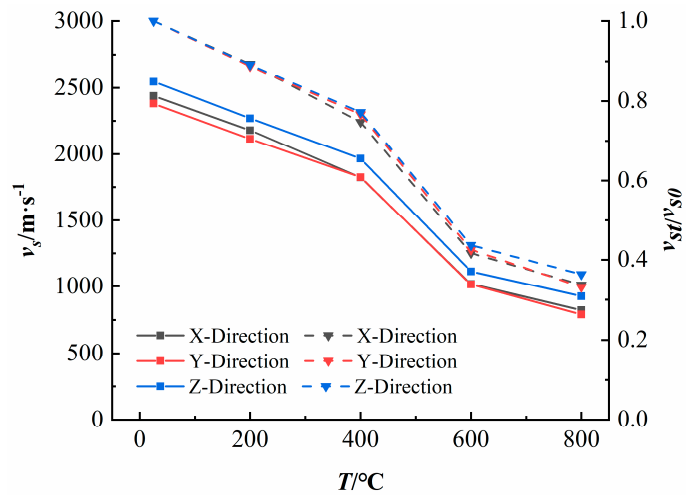


Figure 9. Variation in transverse wave velocity of granite with different temperatures in different sampling directions.

The law of the variation in wave velocity with different temperatures in the three orthogonal directions of granite can be summarized as follows: at room temperature, the Z-direction wave velocity was the highest, and the Y-direction wave velocity was the lowest. As the heating temperature increased, the longitudinal wave velocity of granite, in the first three sampling directions before 400 °C, decreased rapidly, and the Z direction had a faster deceleration rate, while the X direction and Y directions had a slower deceleration rate. The difference in the longitudinal wave velocity of granite in the three directions decreased rapidly, and the difference in the longitudinal wave velocity was the smallest at 400 °C. For the shear wave velocity, at 200 °C, the reduction rate of granite in the three

directions was basically the same and still significantly different. At 400 °C, the reduction rate of the granite shear wave velocity in the X direction was significantly greater than that in the other two directions, rapidly decreasing to the same level as the shear wave velocity in the Y direction. When the temperature exceeded 400 °C, the variation patterns of the longitudinal and transverse wave velocities of granite in the three directions were basically the same. The wave velocities of granite in the X and Y directions tended to be consistent and significantly lower than those of granite in the Z direction. When the heating temperature reached 800 °C, the relationship between the longitudinal wave velocities of granite in the three directions was the same as that for normal temperatures, but the difference was not significant, while the transverse wave velocities of granite in the Z direction were still significantly greater than those in the other two directions.

In summary, there was a significant difference in the influence of temperature on the longitudinal and transverse wave velocities of granite. At the heating temperatures of 200–400 °C, the longitudinal wave velocity approximately linearly decreased, and the rate of decrease in the longitudinal wave velocity was significantly greater than that in the transverse wave velocity. At 600 °C, the longitudinal wave velocity continued to decrease rapidly, while the transverse wave velocity decreased significantly faster than at 400 °C. As the temperature continued to rise, the rate of the wave velocity decrease slowed down. There was a significant change in the wave velocity of granite before and after 400 °C.

3.4. Changes in Uniaxial Compressive Strength and Elastic Modulus

Figure 10 illustrates the relationship between the uniaxial compressive strength of granite and temperature variation. As shown in the Figure 10, the uniaxial compressive strength of granite decreased with an increasing temperature, but the uniaxial compressive strength of granite sampled in the different directions shows different trends: At room temperature, the Z-direction granite had the highest strength, followed by the X-direction granite, and the Y-direction granite had the lowest strength. As the temperature increased from room temperature to 400 °C, the strength of the granite decreased. The difference in the uniaxial compressive strength of granite in the three directions rapidly decreased within this temperature range, and the strength of granite in the Z direction was slightly greater than that in the X and Y directions. When the temperature increased to 600 °C, the strength of granite in the three directions decreased rapidly, and the strength of granite in the Y direction was relatively lower than that in the other two directions. As the temperature continued to rise, after the high temperature increased to 800 °C and 1000 °C, the strength differences in the three directions gradually disappeared and tended to be consistent.

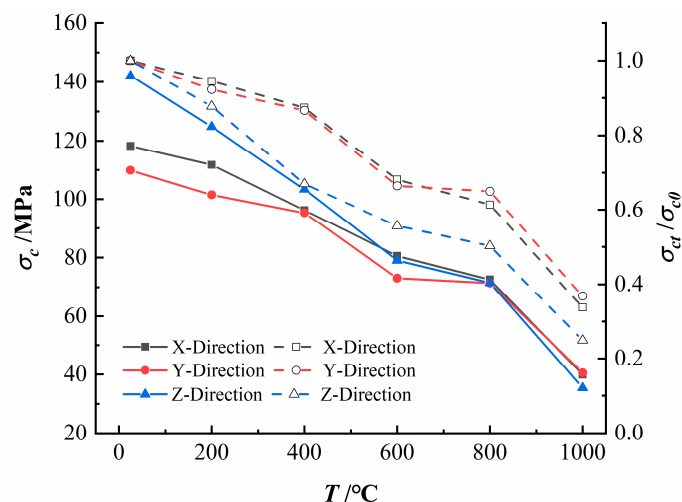


Figure 10. Temperature-dependent variation in the uniaxial compressive strength of granite under different sampling directions.

For samples obtained from different sampling directions, within the temperature range of room temperature to 600 °C, the changes in the strength of granite in the X and Y directions were relatively similar, both showing slight decreases in the uniaxial compressive strength after being subjected to temperatures below 400 °C. At 400 °C, the strength in the X and Y directions decreased by 12.62% and 13.32%, respectively, compared to that in the room-temperature state. As the temperature rose to 600 °C, the strength in the X and Y directions decreased by 31.89% and 33.57%, respectively, compared to that in the room-temperature state. However, the variation trend of granite sampled in the Z direction within this temperature range significantly differed. As the temperature increased, the uniaxial compressive strength of granite in the Z direction approximately decreased linearly, and the rate of decrease was much greater than that in the other two sampling directions. At 600 °C, the uniaxial compressive strength of granite in the Z direction decreased by 45.38% compared to that at room temperature. When the heating temperature was higher than 600 °C, the difference in the trend of the uniaxial compressive strength of granite in the three sampling directions gradually decreased, and the rate of strength reduction slowed down in the range of 600–800 °C. At 1000 °C, the strength of granite rapidly decayed to the minimum value, and the uniaxial compressive strength of granite in the X, Y, and Z directions decreased by 66.24%, 63.14%, and 75.08%, respectively, compared to that at room temperature.

Figure 11 shows the relationship between the elastic modulus of granite and temperature variation. The elastic modulus of granite in the X direction was 25.74 GPa at room temperature, which slightly decreased before 400 °C and decreased to 23.14 GPa at 400 °C for a decrease of 10.15% compared to room temperature. When the temperature was above 400 °C, the elastic modulus decreased almost linearly and dropped to 4.75 GPa at 1000 °C, a decrease of 81.54% compared to room temperature. The elastic modulus of granite in the Y direction at room temperature was 23.30 GPa, which was slightly lower than that in the X direction. As the temperature increased, the rate of decrease in the elastic modulus gradually accelerated. At 400 °C, the elastic modulus of granite in the Y direction was 20.03 GPa, which was 14.06% lower than that at room temperature. When the temperature increased to 800 °C, the rate of decrease in the elastic modulus slowed down compared to that at 600 °C. When the heating temperature exceeded 800 °C, the elastic modulus rapidly decreased again. At 1000 °C, the elastic modulus of the granite decreased to 4.62 GPa, which was 80.26% lower than that at room temperature. The elastic modulus of granite in the Z direction at room temperature was 25.88 GPa, which was the maximum value in the three sampling directions. As the temperature increased, the elastic modulus of the granite increased slightly at 200 °C. Within the temperature range of 200–600 °C, the elastic modulus decreased approximately linearly, with the fastest rate of decrease among the three directions. Compared to those at room temperature, the reduction amplitudes at 400 °C and 600 °C were 18.85% and 39.67%, respectively, which were significantly greater than those in the other two directions. As the temperature continued to increase, the variation in the elastic modulus with different temperatures was approximately in the Y direction. At 1000 °C, the elastic modulus decreased to 4.16 GPa, a decrease of 83.94% compared to room temperature.

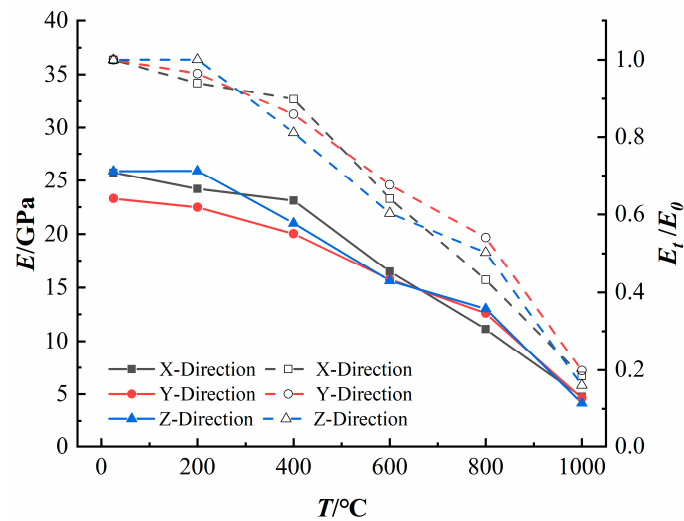


Figure 11. Temperature variation pattern of granite E in different sampling directions.

3.5. Changes in Cohesion and Internal Friction Angle

Cohesion and the internal friction angle are parameters of rock shear strength, where the internal friction angle reflects the friction characteristics of a rock. The main influencing factors include the material, mineral composition, porosity, etc., of the rock, while cohesion is an indicator of the internal bonding strength of a rock and is related to the mineral particle size, bonding composition, and bonding degree.

Figure 12 shows the variation trend of the internal friction angle of the rock samples in the different sampling directions with an increasing temperature, as well as the normalized internal friction angle with temperature variation. As shown in Figure 12, the internal friction angle of the rock samples in all three directions showed an overall upwards trend with an increasing temperature, indicating that a high temperature slightly increased the internal friction angle of the granite. Under normal temperature conditions, the internal friction angles of the granite in the three directions were arranged in descending order: Y direction > X direction > Z direction. As the temperature increased to 800 °C, the internal friction angle of the X-direction rock sample first increased, then decreased, and then increased again, while the internal friction angle of the Y-direction rock sample first slightly decreased. After 400 °C, the internal friction angle of the Z-direction rock sample increased at a relatively rapid rate, and it approximately linearly increased until it slightly decreased above 600 °C. When the temperature increased to 1000 °C, the internal friction angle of the rock samples in the three directions decreased to different degrees, but the values were still greater than those of the original state. Specifically, at 1000 °C, the feldspar melts formed a smooth glaze surface, resulting in a decrease in the friction coefficient and a decrease in friction between the mineral components. However, due to the high-temperature treatment, a large number of cracks were generated, minerals were broken, and small mineral particles filled the cracks. The friction characteristics of the particles were improved compared to those in the initial state. Therefore, compared with that at 800 °C, the internal friction angle at 1000 °C decreased but was still greater than that in the initial state.

Figure 13 shows the variation in cohesion with different temperatures in the rock samples from the different sampling directions, as well as the trend in cohesion with an increasing temperature after normalization. Although the cohesion of the rock samples from all three sampling directions decreased overall with an increasing temperature, there were differences in the variation patterns of the different temperature ranges. At 200 °C, the cohesion of the rock samples in all three sampling directions showed a decreasing trend, but the rate of decrease in the Y direction was significantly lower than that in the other two sampling directions. At 400 °C, the cohesion of the rock samples in the X direction slightly increased, while the cohesion of the rock samples in the other two directions continued to decrease. The decrease in cohesion of the rock samples in the Z direction was much

greater in this temperature range than in the other two directions. As the temperature continued to increase, the cohesion of the rock samples in the three directions decreased steadily, and the rates of decrease were relatively close. The effects of temperature on the cohesion of the rock samples in the different sampling directions tended to be consistent. The normalized results reveal that the cohesion of the Z-direction rock sample was more sensitive to a high-temperature response than was that of the other two directions. As the temperature increased, the decrease in cohesion of the Z-direction rock sample relative to the initial state was significantly greater than that of the other two directions.

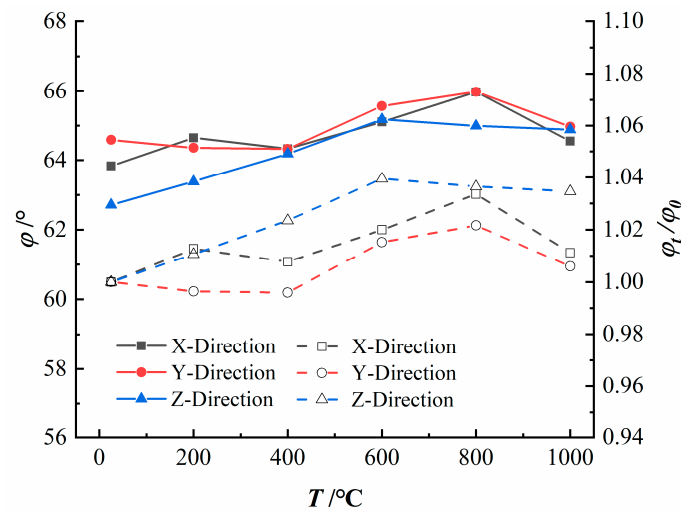


Figure 12. Temperature-dependent variation in the internal friction angle of granite in different sampling directions.

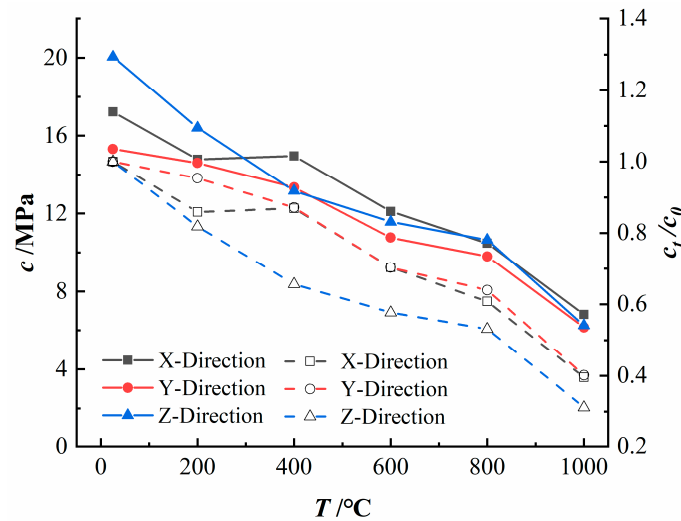


Figure 13. The variation law of granite cohesion with different temperatures in different sampling directions.

3.6. Anisotropic Variation

According to Formula (1), proposed by Birch et al. [29], the anisotropy indexes of rock physical and mechanical properties are obtained.

$$R_S = \frac{(S_{max} - S_{min})}{S_{mean}} \times 100\% \tag{1}$$

R_S is the anisotropy of a certain physical and mechanical index of granite, S_{max} is the maximum value of this index, S_{min} is the minimum value of this index, and S_{mean} is the average physical and mechanical index of rock samples in all sampling directions.

Figure 14 illustrates the variation of the granite wave velocity anisotropy with different temperatures. At a heating temperature of 200 °C, the granite's anisotropy decreased. This decrease in wave velocity was attributed to the removal of free water and weakly bound water from primary fractures within the granite. On the other hand, an increase in the temperature led to the expansion and mutual compression of mineral particles, which could cause some cracks to be compressed or even disappear. This phenomenon was random and irregular, resulting in a decrease in the anisotropy of the granite wave velocity at 200 °C. As the heating temperature increased, the anisotropy of the two types of rocks gradually increased. New microcracks were generated and propagated along the weakest surface of the mineral crystals and might have also connected to form large cracks. At 400 °C, the anisotropy of the granite wave velocity increased. At 600 °C, the anisotropy of the longitudinal wave velocity in the granite reached its maximum value, which was significantly greater than that at room temperature. After heating above 800 °C, the anisotropy of the longitudinal wave velocity in the granite decreased but was still greater than that in the normal temperature state. It can be inferred that temperatures above 400 °C can amplify the anisotropy of the longitudinal wave velocity in granite.

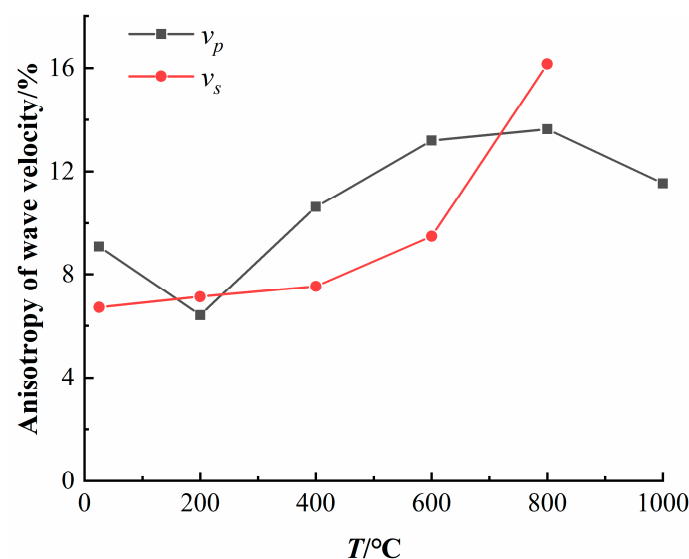


Figure 14. The variation law of wave velocity anisotropy with different temperatures.

The trend of the peak deviatoric stress anisotropy with respect to temperature under different confining pressure conditions is shown in Figure 15. Under uniaxial compression conditions, the peak deviatoric stress anisotropy first increased and then decreased with temperature. In the temperature range of 200~600 °C, the anisotropy of the peak deviatoric stress increased compared to that at room temperature, indicating that within this temperature range, thermal damage within the granite leads to a more pronounced anisotropy of the peak stress in the granite. When the heating temperature exceeded 600 °C, the anisotropy of the peak deviatoric stress in the granite rapidly deteriorated, and the difference in the peak deviatoric stress in each sampling direction decreased. As the confining pressure increased, it could be observed that the confining pressure can significantly reduce the anisotropy of the granite peak deviatoric stress. At various temperature levels, the anisotropy of the granite did not change much compared to that at room temperature, indicating that under the combined influence of a confining pressure and temperature, the peak deviatoric stress of granite can still show a certain degree of anisotropy.

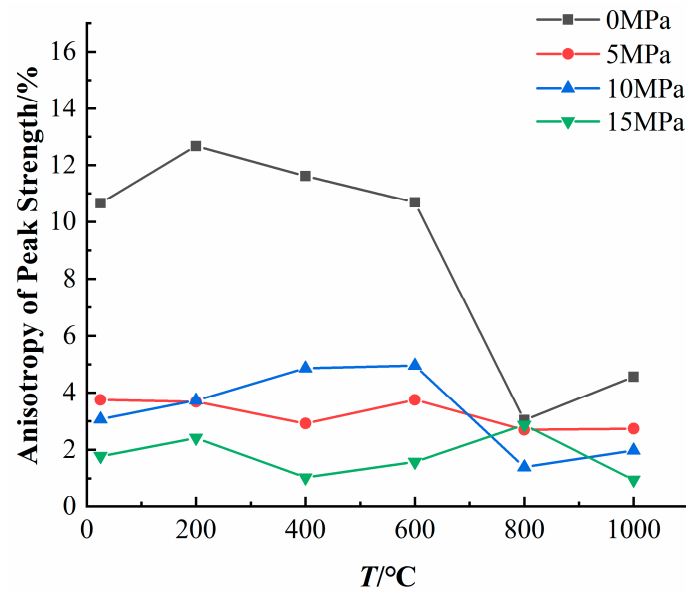


Figure 15. Changes in peak stress anisotropy with different temperatures.

Figure 16 shows the variation in the anisotropy of the elastic modulus with different temperatures. Under various confining pressure conditions, the anisotropy of the granite elastic modulus remained basically unchanged with different temperatures, and the anisotropy of the elastic modulus first increased and then decreased with an increasing temperature. The degree of anisotropy reached its maximum value at 400 °C, and as the temperature continued to rise, the degree of anisotropy began to decrease. As the confining pressure increased, the degree of anisotropy gradually decreased, indicating that a confining pressure can constrain the expression of anisotropy in the elastic modulus of granite. Under uniaxial conditions and a confining pressure of 5 MPa, there was little difference in the anisotropy of the elastic modulus between 200 °C and 400 °C. At the confining pressures of 10 MPa and 15 MPa, the anisotropy of the elastic modulus increased at 400 °C, compared to that at 200 °C. This phenomenon indicates that the confining pressure has a slight enhancing effect on the anisotropy in the temperature range of 200~400 °C.

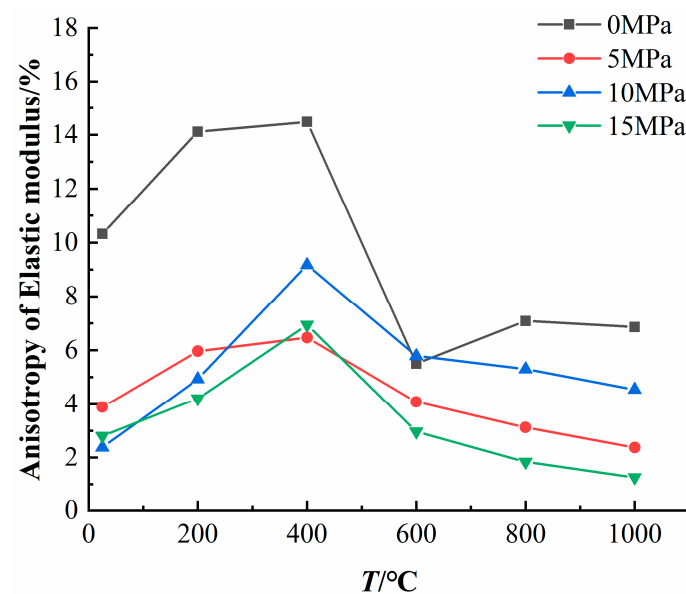


Figure 16. Temperature-dependent variation in the anisotropy of the elastic modulus.

3.7. Destructive Forms

The failure mode of granite is influenced by three factors: temperature, sampling direction, and confining pressure. Figure 17 shows photos of the failure modes of the granite in the three sampling directions under different temperatures and confining pressures. As the temperature and confining pressure increased, in the same sampling direction, the failure mode of the rock samples obviously changed from brittle failure to ductile failure. The failure mode of the granite under uniaxial conditions was mostly tensile splitting failure, while under triaxial compression conditions, the failure mode was shear failure. Although the failure modes of the rock samples in the different sampling directions were the same, there were certain differences in the morphology of the fracture surface.



Figure 17. Failure morphology of granite in different sampling directions.

Under uniaxial compression conditions, the initial failure mode of the granite at room temperature was typical axial splitting failure.

The rock sample in the X direction underwent tensile failure along the axial direction, with the failure surface penetrating through the rock sample and no further cracks extending. As the heating temperature increased, the failure mode of the X-direction rock sample remained unchanged from 200 °C to 600 °C, but a high temperature caused the internal particles of the rock sample to become loose, and the number of local splitting surfaces that developed along the axis increased. At the same time, directional cracks that developed along the radial weak plane, observed in the photos of the rock samples heated at 200–600 °C, could also form radial cracks along the weak plane when the sample was damaged. When the heating temperature exceeded 600 °C, local shear failure was observed

at the end of the granite in the X direction. Due to the relatively loose internal structure of the rock sample, lateral bulging was more obvious.

At 200 °C, local cracks along the axial direction appeared near the main fracture surface of the Y-direction rock sample, and there were horizontal cracks generated by the directional development of the original cracks. At 400 °C, due to the friction between the end face of the rock sample and the pressure plate, the failure mode exhibited a fractured cone at the upper end and axial splitting failure at the lower end of the cone. When the heating temperature was higher than 400 °C, the failure mode of rock samples in the Y direction changed to a combination of shear failure and tensile fracture failure. With an increasing heating temperature, additional small axial cracks were observed in the local area, and the lateral bulging phenomenon became more obvious.

The Z-direction rock sample also exhibited tensile splitting failure through the rock sample at heating temperatures of less than 400 °C. However, compared to those in the other two sampling directions, more macroscopic cracks along the axial direction appeared during the Z-direction rock sample failure, which was a manifestation of the directional development of cracks caused by thermal damage at the macroscopic level. As the temperature increased, local shear failure occurred in the Z direction of the rock samples at 600 °C and 800 °C but was still dominated by splitting failure, with a large number of axial cracks appearing. At 1000 °C, the failure mode of the rock samples in the Z direction completely changed to shear failure.

Under triaxial compression conditions, the failure mode of the granite in the different sampling directions was mainly shear failure, and the temperature and confining pressure were the main factors affecting the failure mode. At room temperature, as the confining pressure increased, the granite rock sample bore greater axial pressure, more cracks developed, and the failure surface morphology of the rock sample changed from simple to complex. At 5 MPa, the granite usually had a relatively obvious shear failure surface only, while at 10 MPa and 15 MPa, more derived cracks could be observed near the main failure surface. At 200 °C and 400 °C, as the confining pressure increased, the width of the main failure surface increased. This is because at this temperature stage, the cracks generated by granite thermal damage were mainly intergranular cracks. The confining pressure increased the frictional force between the mineral particles. When shear cracks appeared, the influence of the mineral particles on other surrounding mineral particles increased, leading to an increase in the crack width. When the heating temperature was higher than 400 °C, a large number of transgranular cracks were generated during the thermal damage of the granite at this temperature stage. The strength of the mineral particles decreased after experiencing a high temperature, and a large number of transgranular cracks were connected under high shear stress, forming a macroscopic shear failure surface. The mineral particles broke into a powder form, and the shear surface was smoother and more complete than that of the rock samples below 400 °C. As the confining pressure increased, the constraint force on the mineral particles increased, and the degree of crack closure in the rock sample increased. Therefore, at the same heating temperature, rock samples with higher confining pressures are more complete when damaged. Usually, only one main failure surface appears, and the development of local short cracks is significantly reduced.

4. Discussion

The relationships between the three sampling directions and the dominant development direction of cracks were analyzed through crack quantification. The quantitative statistical method for determining crack density refers to Gao et al. [30]. The specific steps are as follows: (1) To present the cracks in the sample after heat treatment more clearly, the cracks in the light microscopic images were extracted and reconstructed. (2) A circular analysis area was selected from the microscopic crack map, a reasonable reference line was used to determine the density, and the microscopic cracks were divided. (3) The microcrack density of the thermally cracked rocks was quantified using the crack density statistical method.

In this article, we selected a circular analysis area with a diameter of 2.04 mm to analyze the distribution characteristics of microcracks in the entire cross-section of the sample as much as possible. According to the microscopic crack density statistical method, we set 13 reference lines, numbered 1–13, with a spacing of 150, as shown in Figure 18 (μm). The length of each reference line is shown in Table 1.

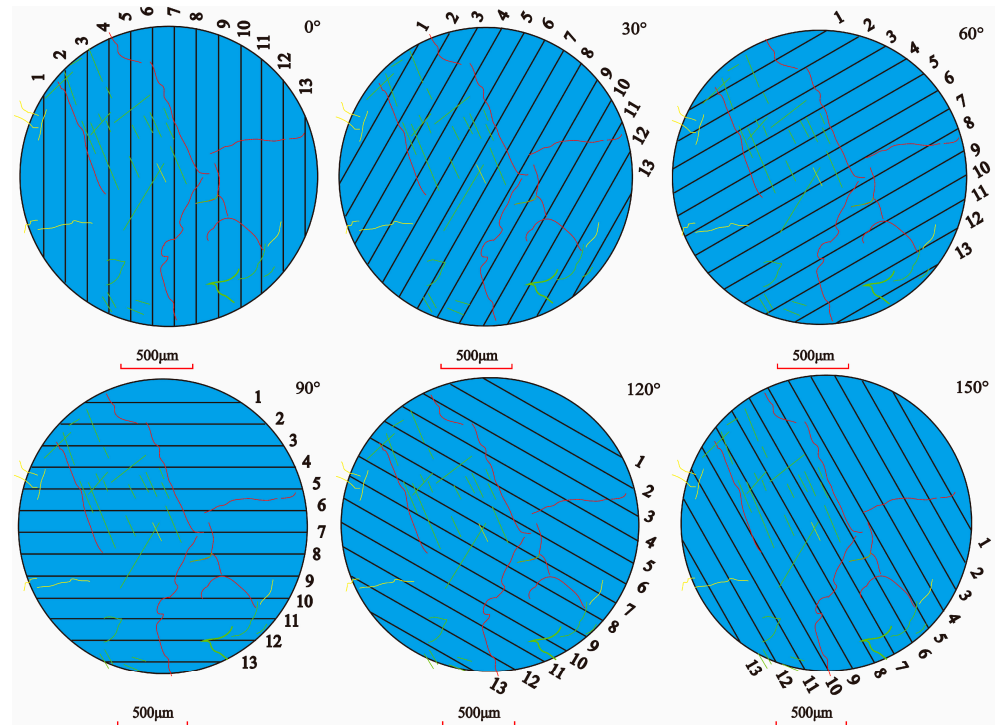


Figure 18. Schematic diagram of the reference line setting and statistical methods.

Table 1. Reference line length.

Reference Line Number	1	2	3	4	5	6	7	8	9	10	11	12	13
Length/mm	0.83	1.31	1.60	1.79	1.93	2.02	2.04	2.04	1.98	1.88	1.71	1.45	1.11

The number of intersection points between each reference line and the microscopic cracks were counted, and the points were divided by the length of each reference line to obtain the density of microscopic cracks on each reference line. The calculation formula for the microscopic crack density LMD is as follows:

$$LMD = \frac{N}{L} \quad (2)$$

In this formula, N is the number of microcracks on the reference line that intersect with the reference line, and L is the length of the reference line.

Using the vertical state of the reference line as the initial level, the line rotates clockwise, and the nonuniformity of the distribution of microcracks at 0° , 30° , 60° , 90° , 120° , and 150° is studied.

According to the above method, the crack distribution status of the rock samples from the three sampling directions was analyzed after different temperature treatments, and the average microcrack density of 13 reference lines was calculated at the 0° , 30° , 60° , 90° , 120° , and 150° reference line angles. When drawing, 30° is taken as the interval, and the reference line angle range is 0° to 180° , which is mapped to the range of 180° to 360° . A

polar coordinate graph of the reference line angle microscopic crack density was drawn, as shown in Figure 18.

Figure 19 shows the distribution of the crack density on the granite cross-sections in the three sampling directions under room-temperature conditions. The rock samples were sampled along the X and Y directions. In the initial state, the distribution of primary cracks on the cross-section of the rock sample was significantly greater in one direction than in other directions. When turning from the angle with the lowest crack density to the angle with the highest crack density, the crack density showed an increasing trend from small to large; this also indicates that there was an advantageous direction of crack distribution on the cross-section of the rock samples in the X and Y directions. However, there was no obvious dominant distribution direction of the crack density on the cross-section of the rock samples sampled along the Z direction, and when rotating from the direction of minimum crack density to the direction of maximum crack density, the crack density did not follow the law of numerical increase. The distribution of the crack density was relatively chaotic, and no obvious trends were observed. Based on these findings, we can determine that the X and Y directions are perpendicular to the dominant crack development direction, while the Z direction is parallel to the dominant crack development direction.

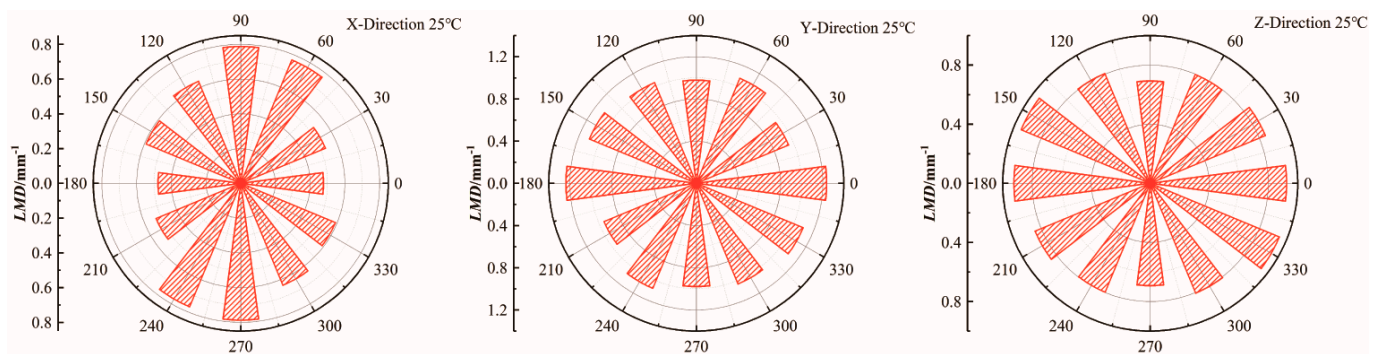


Figure 19. Distributional pattern of cracks on the cross-section of rock samples in different sampling directions at room temperature.

Figures 20 and 21 show the distributional patterns of cracks on the cross-sections of the granite samples taken in the three sampling directions after heating at 400 °C and 800 °C, respectively. At 400 °C, cracks in the cross-sections of the granite samples taken along the X and Y directions developed extensively along the preferred direction, and the density of cracks showed a monotonically increasing trend from small to large, indicating that hot cracks are derived and developed along a certain direction at this temperature. After heating to 800 °C, as a large number of microscopic cracks were generated, developed, and penetrated, the dominant direction of crack development became unclear, and the density of cracks in most directions was high. Thermal damage weakened the anisotropy of the crack distribution in the X and Y directions of the rock samples. For the rock samples sampled along the Z direction, as the heating temperature increased to 400 °C, the crack density increased. However, the pattern of crack-density increase with respect to the angle was relatively chaotic, with the highest crack density occurring in the 30° and 90° directions and the lowest crack density occurring in the 0° and 120° directions. There was no obvious pattern in the distribution of crack density. When the temperature increased to 600 °C and 800 °C, severe physical and chemical changes occurred inside the rock sample, and a large number of microscopic cracks were generated and interconnected to form a crack network. Therefore, the numerical value of the crack density changes relatively little with the reference line angle at lower temperatures, and there is no obvious direction for crack development.

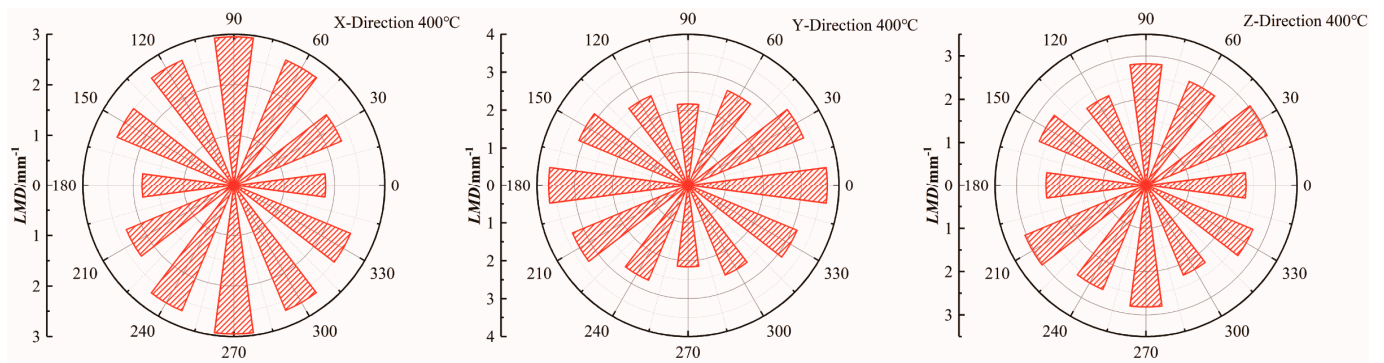


Figure 20. Distributional pattern of cracks on the cross-section of rock samples in different sampling directions above 400 °C.

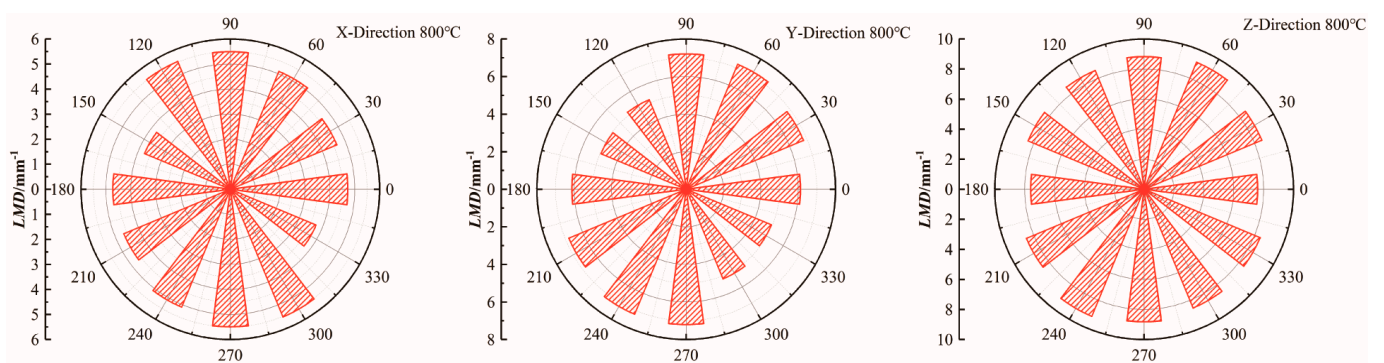


Figure 21. Distributional pattern of cracks on the cross-section of rock samples in different sampling directions above 800 °C.

Through the quantification of thermally induced microcracks and an analysis of the anisotropy of microcrack distribution, it can be seen that the changes in the macroscopic physical and mechanical properties of granite are closely related to the development of microcracks. The strength and deformation characteristics of granite exhibit obvious anisotropy, and the changes in the mechanical indicators of the rock samples with different sampling directions and temperatures reflect the directional development of microcracks at the macroscopic level. At room temperature, the rock samples parallel to the dominant direction of crack development had the lowest crack density in the cross-section, thus exhibiting the best mechanical properties. As the temperature increased to 400 °C, a large number of thermal cracks generated inside the granite developed in the dominant direction, leading to a significant increase in the anisotropy of the physical and mechanical properties of the granite. Under uniaxial compression conditions, the rock samples taken perpendicular to the dominant direction of the cracks produced radial cracks near the main failure surface, while the rock samples taken parallel to the dominant direction of the cracks produced more axial cracks. When the temperature increased to 800 °C and 1000 °C, due to the extensive development and interconnected connection of thermal cracks, microcracks in all directions were extensively developed, and the distribution of microcracks tended to be uniform, which greatly weakened the anisotropy of the physical and mechanical properties of the granite.

5. Conclusions

After subjecting granite samples to high-temperature treatment, a series of physical and mechanical tests were conducted along various sampling directions. This study focused on analyzing the impact of anisotropy on alterations in the physical and mechanical properties of the samples. The findings lead to the following conclusions:

- (1) Temperature can cause significant changes in the appearance and morphology of granite, with a color transition from gray-white to white. Temperatures above 800 °C can cause granite to transform into flesh red. High temperatures above 400 °C can amplify the anisotropy of longitudinal and transverse wave velocities in granite. A temperature of 400 °C is the threshold temperature at which the physical properties of granite change with temperature. Quartz undergoes a phase transition at 573 °C, resulting in significant changes in mechanical properties between 400 °C and 600 °C and a decrease in the peak strength and elastic model. Under the same temperature conditions, granite sampled parallel to the dominant direction of cracks had the best mechanical properties and was more sensitive to temperature.
- (2) There are differences in the crack density on granite cross-sections in different sampling directions. As the temperature increases, the difference in the crack density increases. The development of thermal damage cracks in granite is advantageous. High-temperature actions can cause a large number of mineral microcracks to develop in granite. Temperatures below 400 °C increase the anisotropy of granite. After exposure to higher temperatures, the cracks penetrate each other, the crack density tends to be uniform, the anisotropy weakens, and the confining pressure constrains the mineral particles and compact cracks. The confining pressure will constrain the mineral particles and compact cracks, and anisotropy weakens with the increase in the confining pressure.
- (3) With an increasing temperature and confining pressure, the failure characteristics of granite gradually transition from brittle to plastic failure. When subjected to uniaxial compression, granite is mostly subjected to tensile splitting failure. Rock samples taken perpendicular to the dominant direction of the crack can generate radial cracks near the main failure surface, while rock samples taken parallel to the dominant direction of the crack can generate more axial cracks. As the confining pressure increases, the number of small cracks decreases, and the rock failure mode changes to shear failure.

Author Contributions: Conceptualization, Y.Q. and N.X.; methodology, Y.Q. and L.W.; software, Y.Q. and L.W.; validation, Y.Q. and Q.W.; formal analysis, Y.Q. and Y.G.; investigation, L.W. and G.C.; resources, Y.Q. and N.X.; data curation, Y.Q., L.W. and W.Z.; writing—original draft preparation, Y.Q., Q.W. and Y.G.; writing—review and editing, Y.Q., G.C. and Y.G.; visualization, Y.Q. and L.W.; supervision, Y.Q. and N.X.; project administration, Y.Q.; funding acquisition, N.X. All authors have read and agreed to the published version of the manuscript.

Funding: This research was funded by the National Natural Science Foundation of China (NSFC), under grant no. 42302315 and no. 42230709, And Central Guidance for Local Scientific and Technological Development Funds (YDZJSX20231B016).

Institutional Review Board Statement: Not applicable.

Informed Consent Statement: Not applicable.

Data Availability Statement: Data available on request due to restrictions privacy or ethical.

Acknowledgments: Thank you to the anonymous reviewers for their valuable feedback on the manuscript. The authors thank the National Natural Science Foundation of China (grant no. 42302315 and no. 42230709) and the Central Guidance for Local Scientific and Technological Development Funds (YDZJSX20231B016).

Conflicts of Interest: Author Guanjun Cai was employed by the Beijing Jingneng Geological Engineering Company. The remaining authors declare that the research was conducted in the absence of any commercial or financial relationships that could be construed as a potential conflict of interest.

References

1. Li, C.; Hu, Y.; Meng, T.; Meng, P.; Zhao, Z.; Zhang, C. Experimental study of the influence of temperature and cooling method on mechanical properties of granite: Implication for geothermal mining. *Energy Sci. Eng.* **2020**, *8*, 1716–1728. [[CrossRef](#)]
2. Zhang, F.; Zhao, J.; Hu, D.; Skoczylas, F.; Shao, J. Laboratory investigation on physical and mechanical properties of granite after heating and water-cooling treatment. *Rock Mech. Rock Eng.* **2018**, *51*, 677–694. [[CrossRef](#)]
3. Wang, Z.H.; Su, T.; Konietzky, H.; Tan, Y.L.; Zhou, G.L. Hydraulic properties of Beishan granite after different high temperature treatments. *Bull. Eng. Geol. Environ.* **2021**, *80*, 2911–2923. [[CrossRef](#)]
4. Zuo, J.P.; Wang, J.T.; Sun, Y.J.; Chen, Y.; Jiang, G.H.; Li, Y.H. Effects of thermal treatment on fracture characteristics of granite from Beishan, a possible high-level radioactive waste disposal site in China. *Eng. Fract. Mech.* **2017**, *182*, 425–437. [[CrossRef](#)]
5. Dionísio, A.; Martinho, E.; Pozo-António, J.S.; Braga, M.S.; Mendes, M. Evaluation of combined effects of real-fire and natural environment in a building granite. *Constr. Build. Mater.* **2021**, *277*, 122327. [[CrossRef](#)]
6. Ozguven, A.; Ozcelik, Y. Effects of high temperature on physico-mechanical properties of Turkish natural building stones. *Eng. Geol.* **2014**, *183*, 127–136. [[CrossRef](#)]
7. Bi, J.; Liu, P.; Gan, F. Effects of the cooling treatment on the dynamic behavior of ordinary concrete exposed to high temperatures. *Constr. Build. Mater.* **2020**, *248*, 118688. [[CrossRef](#)]
8. Morrow, C.; Lockner, D.; Moore, D.; Byerlee, J. Permeability of granite in a temperature gradient. *J. Geophys. Res. Solid Earth* **1981**, *86*, 3002–3008. [[CrossRef](#)]
9. Chaki, S.; Takarli, M.; Agbodjan, W.P. Influence of thermal damage on physical properties of a granite rock: Porosity, permeability and ultrasonic wave evolutions. *Constr. Build. Mater.* **2008**, *22*, 1456–1461. [[CrossRef](#)]
10. Sun, Q.; Zhang, W.; Xue, L.; Zhang, Z.; Su, T. Thermal damage pattern and thresholds of granite. *Environ. Earth Sci.* **2015**, *74*, 2341–2349. [[CrossRef](#)]
11. Yang, S.Q.; Ranjith, P.G.; Jing, H.W.; Tian, W.L.; Ju, Y. An experimental investigation on thermal damage and failure mechanical behavior of granite after exposure to different high temperature treatments. *Geothermics* **2017**, *65*, 180–197. [[CrossRef](#)]
12. Zhu, S.; Zhang, W.; Sun, Q.; Deng, S.; Geng, J.; Li, C. Thermally induced variation of primary wave velocity in granite from Yantai: Experimental and modeling results. *Int. J. Therm. Sci.* **2017**, *114*, 320–326. [[CrossRef](#)]
13. Zhang, W.; Sun, Q.; Zhang, Y.; Xue, L.; Kong, F. Porosity and wave velocity evolution of granite after high-temperature treatment: A review. *Environ. Earth Sci.* **2018**, *77*, 350. [[CrossRef](#)]
14. Heuze, F.E. High-temperature mechanical, physical and thermal properties of granitic rocks—A review. *Int. J. Rock Mech. Min. Sci. Geomech. Abstr.* **1983**, *20*, 3–10. [[CrossRef](#)]
15. Liu, S.; Xu, J. An experimental study on the physico-mechanical properties of two post-high-temperature rocks. *Eng. Geol.* **2015**, *185*, 63–70. [[CrossRef](#)]
16. Zhao, Z.; Liu, Z.; Pu, H.; Li, X. Effect of thermal treatment on Brazilian tensile strength of granites with different grain size distributions. *Rock Mech. Rock Eng.* **2018**, *51*, 1293–1303. [[CrossRef](#)]
17. Chen, S.; Yang, C.; Wang, G. Evolution of thermal damage and permeability of Beishan granite. *Appl. Therm. Eng.* **2017**, *110*, 1533–1542. [[CrossRef](#)]
18. Ma, T.; Zhu, G.; Peng, N.; Qiu, Y.; Liu, Y.; Zou, J. Physical-mechanical properties and thermal-induced damage of granite after high-temperature pretreatment. *Arab. J. Geosci.* **2021**, *14*, 1449. [[CrossRef](#)]
19. Kumari, W.G.P.; Ranjith, P.G.; Perera, M.S.A.; Chen, B.K. Experimental investigation of quenching effect on mechanical, microstructural and flow characteristics of reservoir rocks: Thermal stimulation method for geothermal energy extraction. *J. Pet. Sci. Eng.* **2018**, *162*, 419–433. [[CrossRef](#)]
20. Xu, X.L.; Karakus, M. A coupled thermo-mechanical damage model for granite. *Int. J. Rock Mech. Min. Sci.* **2018**, *103*, 195–204. [[CrossRef](#)]
21. Shang, X.; Zhang, Z.; Xu, X.; Liu, T.; Xing, Y. Mineral composition, pore structure, and mechanical characteristics of pyroxene granite exposed to heat treatments. *Minerals* **2019**, *9*, 553. [[CrossRef](#)]
22. Chen, Y.L.; Ni, J.; Shao, W.; Azzam, R. Experimental study on the influence of temperature on the mechanical properties of granite under uni-axial compression and fatigue loading. *Int. J. Rock Mech. Min. Sci.* **2012**, *56*, 62–66. [[CrossRef](#)]
23. Zhu, Z.; Tian, H.; Mei, G.; Jiang, G.; Dou, B.; Xiao, P. Experimental investigation on mechanical behaviors of Nanan granite after thermal treatment under conventional triaxial compression. *Environ. Earth Sci.* **2021**, *80*, 46. [[CrossRef](#)]
24. Alneasan, M.; Alzo'ubi, A.K. Temperature Effect on the Fracture Behavior of Granite Under Three Loading Modes (I, I/II, and II). *Rock Mech. Rock Eng.* **2023**, *56*, 2197–2211. [[CrossRef](#)]
25. Wang, Z.; Zhou, G.; Ge, X. Experimental study on damage characteristics of Beishan granite under single loading and multiple loading with AE techniques. *Sci. Rep.* **2023**, *13*, 8767. [[CrossRef](#)] [[PubMed](#)]
26. Zheng, Y.; Zhang, L.; Wu, P.; Guo, X.; Li, M.; Zhu, F. Physical and Mechanical Properties and Damage Mechanism of Sandstone at High Temperatures. *Appl. Sci.* **2024**, *14*, 444. [[CrossRef](#)]
27. Fan, L.F.; Wu, Z.J.; Wan, Z.; Gao, J.W. Experimental investigation of thermal effects on dynamic behavior of granite. *Appl. Therm. Eng.* **2017**, *125*, 94–103. [[CrossRef](#)]
28. He, L.; Yin, Q.; Jing, H. Laboratory Investigation of Granite Permeability after High-Temperature Exposure. *Processes* **2018**, *6*, 36. [[CrossRef](#)]

29. Birch, F. The velocity of compressional waves in rocks to 10 kilobars, part 2. *Elastic Prop. Equ. State* **1988**, *26*, 91–116.
30. Gao, J.; Xi, Y.; Fan, L.; Du, X. Real-time visual analysis of the microcracking behavior of thermally damaged granite under uniaxial loading. *Rock Mech. Rock Eng.* **2021**, *54*, 6549–6564. [[CrossRef](#)]

Disclaimer/Publisher’s Note: The statements, opinions and data contained in all publications are solely those of the individual author(s) and contributor(s) and not of MDPI and/or the editor(s). MDPI and/or the editor(s) disclaim responsibility for any injury to people or property resulting from any ideas, methods, instructions or products referred to in the content.